Eur. J. Mineral., 37, 829–840, 2025 https://doi.org/10.5194/ejm-37-829-2025 © Author(s) 2025. This work is distributed under the Creative Commons Attribution 4.0 License.





Kayupovaite, Na₂Mn₁₀[(Si₁₄Al₂)O₃₈(OH)₈]·7H₂O – a new stilpnomelane-related mineral from the Ushkatyn-III deposit, Kazakhstan

Oleg S. Vereshchagin¹, Sergey N. Britvin^{1,2}, Aleksey I. Brusnitsyn¹, Anastasiia K. Shagova¹, Elena N. Perova¹, Igor V. Pekov³, Vladimir V. Shilovskikh¹, Natalia S. Vlasenko¹, Evgeniya Y. Avdontseva¹, Natalia V. Platonova¹, and Vladimir N. Bocharov¹

¹Saint Petersburg State University, Saint Petersburg, Universitetskaya Emb. 7/9, 199034, Russia
 ²Kola Science Center, Russian Academy of Sciences, Apatity, Fersman Str. 14, 184200, Russia
 ³Faculty of Geology, Moscow State University, Leninskie Gory, 119991 Moscow, Russia

Correspondence: Oleg S. Vereshchagin (o.vereshchagin@spbu.ru)

Received: 11 August 2025 - Revised: 19 September 2025 - Accepted: 24 September 2025 - Published: 3 November 2025

Abstract. Kayupovaite, with the idealized formula Na₂Mn₁₀[(Si₁₄Al₂)O₃₈(OH)₈]·7H₂O, is a new mineral named in honor of Maria Mikhailovna Kayupova (1921–1980), the mineralogist of the Satpaev Institute of Geological Sciences (Alma-Ata, USSR) who studied the Ushkatyn-III complex baryte-lead/iron-manganese deposit, Karagandy Province, Kazakhstan, the type of locality of the described mineral. Kayupovaite forms coarse lamellar (typically bent and split), light-gray, greasy luster crystals up to $0.2 \times 0.15 \times 0.01$ mm in size, combined into radial, scaly, or lamellar aggregates up to $3 \times 3 \times 0.5$ cm and embedded in a calcite-rhodonite matrix. Optically, in transmitted light, kayupovaite is colorless, with undulatory extinction due to the crystal curvature. It is non-pleochroic and biaxial (-), with α of 1.551(4) and $\beta = \gamma 1.586(2)$, $2V_{\text{meas}} = 3 \pm 1^{\circ}$. Kayupovaite is monoclinic and of space group C_2/c , with a = 24.9149(9), b = 16.4343(5), c = 22.3974(7) Å. $\beta = 94.408(3)^{\circ}$, $V = 9143.7(5) \text{ Å}^3$, and Z = 8. The strongest lines of the powder X-ray diffraction pattern (d in Å (I) (hkl) are as follows: 12.34(100)(200), 3.45(8)(71 – 1), 3.09(8)(800), 2.85(100)(121), 2.5946(12)(714), 2.642(11)(354), 2.614(7)(40 - 8), and 2.414(7)(554). The Raman spectrum of kayupovaite contains the following bands (cm⁻¹): 3635 and 3560 (O-H stretching vibrations of OH groups and H₂O molecules); 1041, 768, 742, and 717 (Si-O and Al-O stretching modes); 657, 532, 499, 460, 405, 374, and 333 (Mn-O stretching and Si-O-Si modes); and 304, 291, 224, 157, and 100 (lattice modes). The absorption bands of the infrared spectrum are as follows (cm⁻¹): 3629, 3511, and 3390 (O-H stretching vibrations of OH groups and H₂O molecules); 1640 (H₂O bending vibrations); 1020 (Si–O stretching vibrations); 778 (^{IV}Al–O stretching vibrations); 724 (Mn–O–H bending mode); 651 (O–Si–O bending mode); and 459 (Mn²⁺–O stretching vibrations). The empirical formula of kayupovaite, calculated on the basis of (O + OH) = 46 atoms per formula unit, is $(Na_{0.91}K_{0.46}Ca_{0.14})_{\Sigma 1.51}(Mn_{9.29}^{2+}Mg_{0.89}Zn_{0.02})_{\Sigma 10.20}[(Si_{14.28}Al_{1.61})_{\Sigma 15.89}O_{38}(OH)_8] \cdot 7.23H_2O. \ The \ mineral \ below 1.51Mg_{0.29}(CH)_{10.20}(CH)_{10$ longs to the group of modulated manganese phyllosilicates and is structurally related to stilpnomelane. The absence of iron in the mineral is a result of oxidative Mn-Fe fractionation during the formation of braunite-rich Mn ores.

1 Introduction

A sample consisting of Mn-rich calcite and rhodonite with a layer (up to 3 cm thick) of an unidentified light-gray mineral was found in 2018 on the bottom of the open pit operating at the Ushkatyn-III complex baryte-lead/iron-manganese deposit in Karagandy Province, Kazakhstan (48°16′06″ N; 70°10′43″ E). Subsequent detail studies have shown that this mineral is a new species belonging to the modulated manganese phyllosilicates. The mineral, with the idealized formula $Na_2Mn_{10}[(Si_{14}Al_2)O_{38}(OH)_8]\cdot 7H_2O$, was named kayupovaite in honor of Maria Mikhailovna Kayupova (Cyrillic: Мария Михайловна Каюпова; Fig. S1 in the Supplement) (1921-1980), the Soviet mineralogist who worked at the Satpaev Institute of Geological Sciences, Almaty (Alma-Ata), Kazakhstan, for her contributions to the mineralogy of Mn-Fe deposits in central Kazakhstan, including Ushkatyn-III (Kayupova, 1964, 1972, 1974). The mineral, its name, and its symbol (Kyp) have been approved by the Commission on New Minerals, Nomenclature and Classification of the International Mineralogical Association, IMA no. 2022-045. The holotype specimen is deposited at the Mineralogical Museum of the Department of Mineralogy, Saint Petersburg State University, Saint Petersburg, Russia, under catalogue no. ML OF 458.

Modulated manganese phyllosilicates (which are also referred to as double-layer sheet silicate based on miscellaneous nets; e.g., Hawthorne et al., 2019) are characterized by two-dimensional silicate anions of unique topologies induced by the incommensurate relationships between the octahedral and tetrahedral sheets (Liebau, 1985; Guggenheim and Eggleton, 1987; Guggenheim and Eggleton, 1988; Grice and Gault, 1995; Hughes et al., 2004; Krivovichev et al., 2004; Yakovenchuk et al., 2007). Several groups of modulated manganese phyllosilicates can be distinguished based on their chemical composition and powder X-ray diffraction patterns. Among them, stilpnomelanerelated minerals are probably the most widespread and geochemically important. Stilpnomelane-related minerals are layered (alumino)silicates rich in Mn and/or Fe (main octahedral cation), containing Na and/or K (main interlayer cation), significantly enriched in H-bearing groups (OH, H₂O), and characterized by quite similar powder X-ray diffraction patterns (with intense peaks with $d \approx 12 \,\text{Å}$). Stilpnomelane-related minerals are armbrusterite $(Na_6K_5Mn^{3+}Mn_{14}^{2+}(Si_9O_{22})_4(OH)_{10}\cdot 4H_2O),$ $((Ca,K,Na)(Mn^{2+},Fe^{2+})_{10}(Si,Al)_{16}O_{38}(OH)_8 \cdot nH_2O),$ $((K,Na)_4(Mn^{2+},Mg,Zn)_{48}(Si,Al)_{72})$ franklinphilite (O,OH)₂₁₆· 6H₂O), lennilenapeite $(K_7(Mg,Mn^{2+},Fe^{2+},Zn)_{48}(Si,Al)_{72}(O,OH)_{216}.$ $16H_2O),$ parsettensite ((K,Na,Ca)_{7.5}(Mn,Mg)₄₉Si₇₂O₁₆₈(OH)₅₀·nH₂O), and middendorfite (K₃Na₂Mn₅Si₁₂(O,OH)₃₆·2H₂O) (e.g., Pekov et al., 2007; Hawthorne et al., 2019). Kayupovaite $(Na_2Mn_{10}[(Si_{14}Al_2)O_{38}(OH)_8]\cdot 7H_2O)$ is a new

stilpnomelane-related mineral, an Na-dominant analogue of bannisterite.

2 Occurrence

The Ushkatyn-III deposit is located 300 km southwest of Karagandy and 15 km northeast of Zhairem Town, Karagandy Province, Kazakhstan. The Ushkatyn-III deposit was discovered in 1962 and has been operating since 1982 (e.g., Kayupova, 1974; Buzmakov et al., 1975; Rozhnov, 1982; Kalinin, 1985). The deposit is complex: both baryte–lead and iron–manganese ores are present in various parts of it (e.g., Kayupova, 1974; Rozhnov, 1982; Brusnitsyn et al., 2021, 2025). The specimen with kayupovaite was found in the zone of braunite-rich ores (see below). It is the second new mineral discovered at the Ushkatyn-III deposit: gasparite-(La) was recently found by us in hausmannite-rich ores (Vereshchagin et al., 2019).

The deposit is located within the continental paleorift and is composed of a sequence of terrigenous-siliceouscarbonate rocks of the Upper Devonian-Lower Carboniferous age. The eastern part of the deposit is composed of reef limestones containing baryte-galena mineralization. In the western part of the deposit, these rocks are replaced first by detrital nodular-layered limestones containing layers of iron and manganese ores. The reef limestones contain baryte–galena mineralization (baryte–Pb ores), while the organogenic-detrital limestones contain Fe (hematite)-Mn ores (braunite and hausmannite). The productive member has a well-defined cyclic structure, with a rhythmic alternation of limestone layers and ore layers, composed of Fe and/or Mn ores (e.g., Brusnitsyn et al., 2021). Iron and manganese ores are almost always separated either by section or by strike. The thickness of individual layers of Mn ores within the deposits ranges from 0.3 to 8 m (2 m on average), while the thickness of Fe ores does not exceed 1 m. The total thickness of the ore-bearing member varies from 50 to 200 m; the member can be traced over a distance of more than 2.5 km and over a depth up to 1.2 km (Brusnitsyn et al., 2024).

Iron and manganese ores are fine-grained rocks with lenticular-banded and layered textures. The main minerals in iron ores are hematite; calcite; quartz; and small amounts of albite, muscovite, baryte, hydroxylapatite, tilasite, pyrite, and galena. The major minerals of the hausmannite ores are hausmannite, rhodochrosite, calcite, tephroite, manganese members of the humite group (sonolite and alleghanyite), and friedelite. Their accessory minerals are hematite, jacobsite, caryopilite, clinochlore, and pennantite. The braunite ores are composed predominantly of braunite and calcite, with subordinate amounts of quartz and albite. Their typical minor minerals include hematite, kutnohorite, rhodochrosite, friedelite, pennantite, rhodonite, axinite-(Mn), and potassic feldspar (e.g., Kayupova, 1974; Vereshchagin et al., 2019; Brusnitsyn et al., 2024, 2025).

Based on available mineralogical, geochemical, and isotopic data, it was suggested that the deposit was formed during low-grade metamorphism (~ 250 °C, ~ 200 MPa) of metalliferous sediments composed of Fe³⁺ and Mn³⁺/Mn⁴⁺ oxides, carbonates, (alumino)silicates, and organic matter (Brusnitsyn et al., 2024). It is assumed that iron and manganese initially accumulated in the discharge area of hydrothermal solutions seeping into the sea basin along fault zones (e.g., Kayupova, 1974; Rozhnov, 1982; Brusnitsyn et al., 2021). The differentiation of metals occurred with the sequential precipitation of iron (first) and manganese (second) as a result of fluctuations in the physicochemical parameters (temperature, pressure, and oxygen fugacity) of the water mass due to sea level change and/or changes in hydrothermal activity. This process was regularly interrupted, resulting in the formation of a cyclically constructed ore-bearing sequence with alternating ore Fe-Mn layers and limestones (separating them). Key differences in the mineral compositions of two types of manganese ores (braunite vs. hausmannite) were due to the unequal content of reactive organic matter (OM) in the original sediments (Brusnitsyn et al., 2020, 2021, 2024). Braunite ores are formed under oxidizing conditions, while hausmannite ores are formed in a relatively reducing subanaerobic environment. Braunite and hausmannite ore associations should be considered to be "oxidized" and "reduced" facies of metamorphosed manganese deposits, respectively (Brusnitsyn et al., 2020, 2021, 2024, 2025).

Weakly metamorphosed Mn-rich sediments are typical for most of the stilpnomelane-related minerals (except armbrusterite and middendorfite). Stilpnomelane is known from several hundred localities worldwide, among which the banded iron formation (BIF) type is the most important, being present as an indicator of low-grade metamorphic conditions and possible rare Earth element careers (e.g., Haugaard et al., 2017). It is worth noting that most of the stilpnomelane finds have not been confirmed by X-ray diffraction, suggesting that at least some of them may be other stilpnomelane-related minerals. Both bannisterite and parsettensite are known from about 20 localities (see mindat.org) and are typical for low-grade Mn-rich sediments (e.g., Sustavov et al., 1997).

3 General appearance and optical properties

Kayupovaite forms coarse lamellar (typically bent and split) crystals up to $0.1 \times 0.05 \times 0.02$ mm in size, combined into radial, scaly, or lamellar aggregates up to $3 \times 3 \times 0.5$ cm in size and embedded in a calcite–rhodonite matrix (Fig. 1). The mineral is light gray with white streaks and greasy luster. It is non-fluorescent under either short- or long-wave ultraviolet radiation. The Mohs' hardness of kayupovaite is 4; the mineral is brittle with perfect cleavage. The calculated density is $2.76 \, \mathrm{g \, cm^{-3}}$ based on the chemical data (Table 1) and unit cell parameters obtained from single-crystal X-ray diffraction (SCXRD) data (Table 2).

Optical properties of kayupovaite were studied by means of a DLMP polarizing light microscope (Leica, Germany). Kayupovaite is colorless in transmitted light, with undulatory extinction due to crystal curvature. The mineral is biaxial (–), with $\alpha=1.551(4)$, $\beta=\gamma1.586(2)$, and $2V_{\rm meas}=3\pm1^\circ$. The Gladstone–Dale compatibility index 1 (K_p/K_c) is 0.042 (good).

4 Thermal analysis and chemical composition

The differential scanning calorimetry (DSC) and thermogravimetry (TG) curves of kayupovaite (Fig. 2) were obtained using an STA 449 F3 Jupiter instrument (Netzsch, Germany). The analyzed sample ($\sim 2 \,\mathrm{mg}$) was heated (in an oxygen atmosphere) from 30 to 1200 °C at a rate of 10 °C min⁻¹. Kayupovaite has an intense and wide endothermic peak at low temperatures, accompanied by a sharp loss of sample weight. The parameters of this effect for kayupovaite are $t_{\text{max}} = 126 \,^{\circ}\text{C} \, (-4.2 \,\%)$. It is most likely that the rapid weight loss at t = 100-200 °C is caused by the removal of weakly bound water from kayupovaite. A sloping decrease in the level of the DSC and TG curves of the studied mineral is recorded in the region of t > 200 °C. A gradual decrease in mass at higher temperatures is associated with the release of zeolite water, and local inflections on the TG curve correspond to the loss of constitutional water structurally bound in the form of OH groups. Inflections on the TG curve due to a decrease in mass were established at $t = 420 \,^{\circ}\text{C} (-2 \,\%)$ and $t \approx 1000$ °C (-2.5 %). The DSC curve of kayupovaite registers a narrow and intense exothermic effect without changing the mass of the sample at t = 770 °C. The decrease in mass is due to the processes of dehydration. The total weight loss for kayupovaite is 10.7 %, of which 4.2 % is accounted for by crystallization water, and 6.5 % is accounted for by zeolite and constitutional water.

Elemental composition (Table 1, Fig. 3) and morphology (Fig. 1) were studied by means of an S-3400 N (Hitachi, Japan) scanning electron microscope (SEM) equipped with an AzTec Energy X-Max 20 (Oxford Instruments, UK) energy-dispersive X-ray (EDX) and WAVE 500 (Oxford Instruments, UK) wavelength-dispersive X-ray (WDX) spectrometers. The conditions of the analyses were 20 kV (accelerating voltage), 2 nA (beam current), and 20 s (data collection time) for EDX and 20 kV, 5 nA, and 60 s (30 s per element and 30 s background acquisition times) for WDX. The elemental composition of kayupovaite was obtained by EDX during 5×5 to $10 \times 10 \,\mu m$ area scans as higher acquisition time (needed for WDX) led to an increase in K content due to e-beam-induced intra-lattice cation migration typical for stilpnomelane-related minerals (e.g., Plimer, 1977; Dunn et al., 1992). Additionally, Na, K, and Li contents were measured by inductively coupled plasma optical emission spectroscopy (ICP-OES) on an OPTIMA-4300 spectrometer (Perkin-Elmer, USA). The

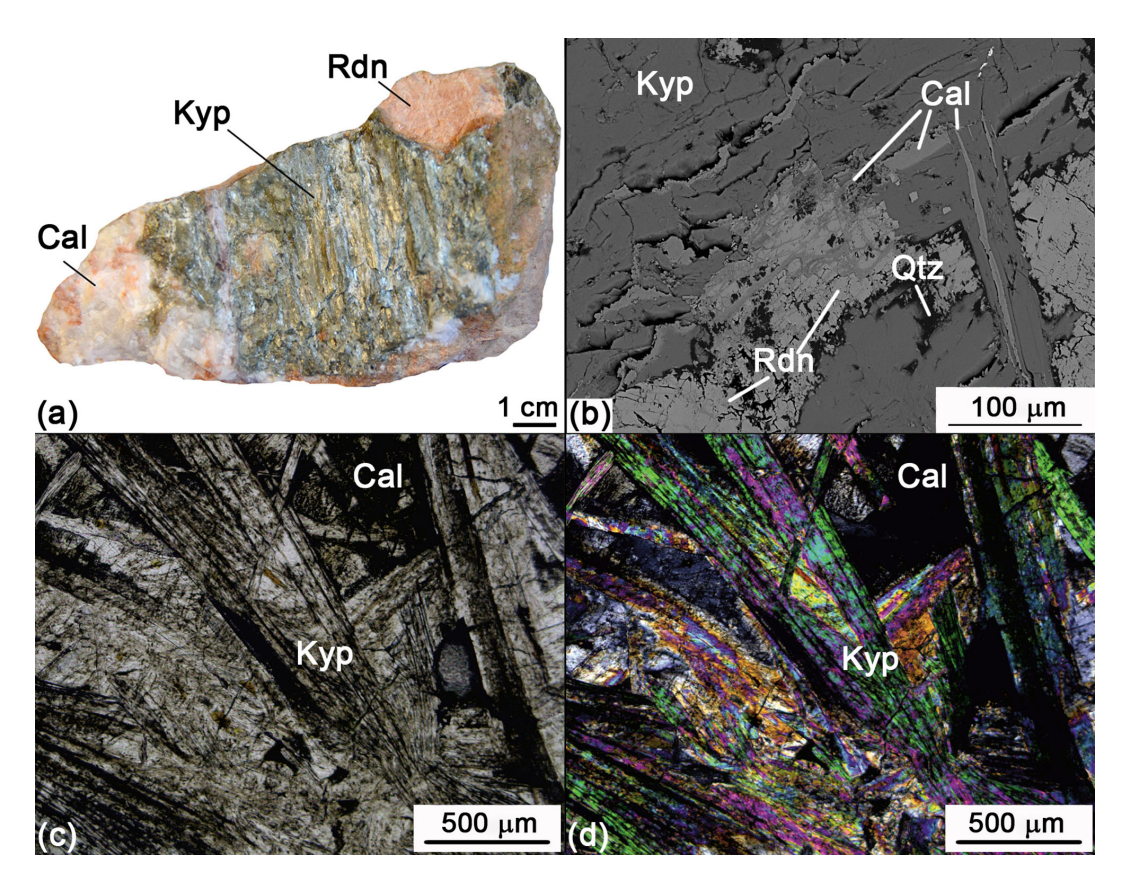


Figure 1. Kayupovaite (Kyp) aggregate in calcite (Cal)—rhodonite (Rdn) rock: (a) hand specimen Ush318-106 – a veinlet made by a parallel-lamellar aggregate of kayupovaite. The sample is oriented nearly parallel to the plane of the vein. (b) Scanning electron microscope—backscatter electron image (SEM BSE) image – calcite veinlets inside kayupovaite aggregate. (c) Parallel-polarized light and (d) cross-polarized light – clusters of lamellar kayupovaite crystals.

Table 1. Chemical data (in wt %) for kayupovaite.

Constituent	Mean	Range	SD (2σ)	Reference material
SiO ₂	45.36	42.30–47.91	3.78	Quartz
Al_2O_3	4.35	3.77-4.94	0.78	Corundum
MnO	34.92	33.30-36.36	2.04	Mn metal
ZnO	0.07	0.00 - 0.22	0.18	Zn metal
MgO	1.88	1.51-2.36	0.68	MgO
CaO	0.42	0.27 - 0.70	0.26	Anhydrite
Na ₂ O	1.49	1.27 - 1.70	0.28	Halite
K ₂ O	1.14	0.78 - 1.36	0.46	Sylvite
H_2O^*	10.7			
Total	100.33			

^{*} From thermal data.

obtained data (Na₂O – 1.64 %, K₂O – 1.08 %, Li – 15 ppm) are close to the corresponding chemical data (Table 1) and indicate that the mineral is virtually Li-free with Na > K. The empirical formula of kayupovaite calculated on the basis of (O + OH) = 46 atoms per formula unit is (Na_{0.91}K_{0.46}Ca_{0.14}) $_{\Sigma 1.51}$ (Mn²⁺_{9.29}Mg_{0.89}Zn_{0.02}) $_{\Sigma 10.20}$ [(Si_{14.28} Al_{1.61}) $_{\Sigma 15.89}$ O₃₈(OH)₈]·7.23H₂O. The simplified formula is

 $(Na,K,Ca)_2(Mn^{2+},Mg)_{10}[(Si,Al)_{16}O_{38})(OH)_8]\cdot 7H_2O$, while the ideal formula is $Na_2Mn_{10}[(Si_{14}Al_2)O_{38}(OH)_8]\cdot 7H_2O$, which requires the following (wt %): $SiO_2 - 43.96$, $Al_2O_3 - 5.33$, MnO - 37.07, $Na_2O - 3.24$, and $H_2O - 10.40$ (total 100).

Table 2. Crystal parameters, data collection, and structure refinement details for kayupovaite.

Crystal data	
Crystal size (mm)	$0.20 \times 0.15 \times 0.01$
Crystal system, space group	Monoclinic, C2/c
a,b,c (Å)	24.9149(9), 16.4343(5), 22.3974(7)
β (°)	94.408(3)
$V(\mathring{A}^3)$	9143.7(5)
Z	8
$D_x (\text{g cm}^{-3})$	2.570
Data collection and refinement	
HKL file type	HKLF5
Radiation	$MoK\alpha \ (\lambda = 0.71073 \text{Å})$
Temperature (K)	296
$2\Theta_{\max}$ (°)	Truncated at 50.00
No. of measured, independent, and observed $(I > 2\sigma(I))$ reflections	45 681, 45 681, 33 479
h, k, l range	$-29 \rightarrow 29, -19 \rightarrow 19, -26 \rightarrow 26$
F(000)	6875
$\mu (\mathrm{mm}^{-1})$	3.10
No. of refined parameters	698
$R_1 [F \ge 4\sigma(F)], wR_2$	0.162, 0.530
Goodness of fit (GoF)	2.35
Data completeness	0.956

Table 3. X-ray powder diffraction pattern of kayupovaite (*d* spacings in Å). The most intense lines are marked in bold.

Imeas	$d_{ m meas}$	Icalc	d_{calc}	h	k	l	Imeas	$d_{ m meas}$	$I_{ m calc}$	$d_{ m calc}$	h	k	l
4	13.85	2	13.71	1	1	0	8	3.09	3	3.11	8	0	0
100	12.34	100	12.42	2	0	0	12	2.85	1	2.852	7	1	4
		3	11.91	1	1	-1			1	2.827	1	5	-4
		2	11.47	1	1	1	4	2.800	3	2.802	1	5	4
3	8.90	1	8.842	1	1	-2			1	2.798	3	5	3
		1	8.482	1	1	2	4	2.761	2	2.769	2	0	-8
2	7.16	2	7.168	3	1	-1	1	2.710	1	2.706	7	3	3
1	6.93	2	6.880	3	1	1	11	2.642	7	2.649	3	5	4
		1	6.661	1	1	-3	7	2.614	4	2.623	4	0	-8
1	5.55	< 1	5.583	0	0	4			1	2.503	5	5	-4
2	5.21	1	5.222	1	3	-1	3	2.487	1	2.489	3	5	5
3	4.61	2	4.618	0	2	4	7	2.414	3	2.420	5	5	4
1	6.47	< 1	6.430	1	1	3	6	2.393	2	2.402	6	0	-8
		1	4.301	1	1	-5	1	2.323	< 1	2.318	8	4	-4
5	4.11	4	4.140	6	0	0	2	2.255	1	2.257	7	5	-4
		1	4.109	0	4	0			1	2.236	6	0	8
		1	3.856	0	4	2	4	2.169	2	2.173	7	5	4
4	3.81	2	3.824	4	2	-4			1	2.160	8	0	-8
3	3.66	< 1	3.655	2	4	2	3	2.010	1	2.016	9	5	-4
2	3.59	1	3.598	4	2	4	2	1.932	1	1.939	9	5	4
		1	3.469	7	1	0			1	1.643	0	10	0
8	3.45	2	3.467	7	1	-1			1	1.623	1	5	-12
		1	3.427	4	4	0			1	1.610	3	5	-12
5	3.37	2	3.389	7	1	1							

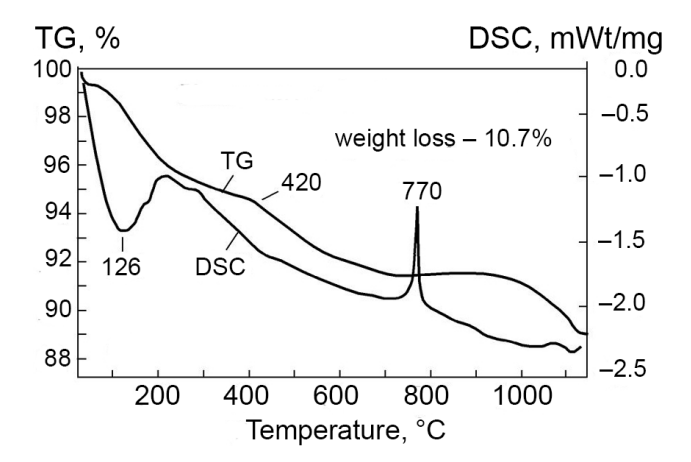


Figure 2. Differential scanning calorimetry (DSC) and thermogravimetric (TG) curves of kayupovaite.

5 X-ray powder diffraction and single-crystal data

X-ray powder diffraction data were obtained using a R-AXIS Rapid II diffractometer (Rigaku, Japan), a curved (cylindrical) imaging plate detector ($r=127.4\,\mathrm{mm}$), $\mathrm{Co}\,\mathrm{K}\alpha$ radiation ($\lambda=1.79021\,\mathrm{\mathring{A}}$), a rotating anode (40 kV, 15 mA) with microfocus optics, Debye–Scherrer geometry, and an exposure time 15 min (Table 3). Because of multiple indexing and the weak intensities of lines, the attempts to refine unit cell parameters based on powder data did not give reliable results (e.g., Dunn et al., 1992). Therefore, theoretical pattern (Table 3) was calculated using CCDC Mercury 2020.3.0 based on structure refinement results.

Single-crystal X-ray diffraction (SCXRD) analysis was performed using an XtaLAB Synergy-S (Rigaku Oxford Diffraction, Japan) diffractometer equipped with a HyPix-6000HE detector with monochromated Mo $K\alpha$ radiation ($\lambda[\text{MoK}\alpha]=0.71073\,\text{Å}$) at 50 kV and 1 mA. More than a hemisphere of three-dimensional data was collected, with a frame width of 0.2°. The data were integrated and corrected for background, Lorentz, and polarization effects. An empirical absorption correction based on spherical harmonics implemented in the SCALE3 ABSPACK algorithm was applied in the CrysAlisPro program. The anisotropic displacement parameters were refined for all atoms.

Kayupovaite crystals are of very poor quality (Fig. 1), and, even with the best selected platelets and applying a narrow frame width (0.2°), the diffraction patterns resemble oblique layered textures rather than single-crystal frames (Fig. 4). That is, altogether, large unit cell parameters and twinning made data reduction, structure solution, and refinement of kayupovaite a challenging task (Table 2). The crystal structure was solved and refined using the SHELX-2018 set of programs (Sheldrick, 2008) and the Olex2 v.1.5 graphical user interface (Dolomanov et al., 2009) based on the HKLF5 file obtained from the twinned platelet ([-100][0-10][001]). The best achieved reliability index after anisotropic refine-

ment was 0.16, but the structure is clearly defined. Atomic positions in [SiO₄] tetrahedra, [MnO₆] octahedra, and Na atoms are the same as in the reported bannisterite structure (Heaney et al., 1992) (Crystallographic Information File; Fig. 5). The bond lengths are of the same order as in bannisterite (Heaney et al., 1992), and, like the latter, the Si–O distances at the hydroxyl-bonded atoms Si13, Si14, and Si15 are substantially elongated (Crystallographic Information File; Fig. 5). All Na sites were refined as Na and were found to have incomplete occupancy. Magnesium partially substitutes manganese in Mn1, Mn2, and Mn4 positions (Crystallographic Information File). Because of poor data quality and low overall Al contents, no attempts were made to refine the Si–Al population; therefore, all tetrahedral units were treated as [SiO₄].

The interstitial complexes of kayupovaite, as well as of other stilpnomelane-related minerals, are based on miscellaneous nets that consist of sheets of octahedrally coordinated Mn²⁺/Fe²⁺/Mg²⁺, with additional alkaliand alkaline-Earth cations (Na/K/Ca) and (H₂O) groups in interlayer (Eggleton, 1972; Guggenheim and Eggleton, 1988; Heaney et al., 1992; Eggleton and Guggenheim, 1994; Hawthorne et al., 2019). It should be noted that the crystal structures of only kayupovaite, bannisterite, and armbrusterite were solved and refined on the basis of SCXRD data, while the crystal structures of all of the other stilpnomelane-related minerals were studied using only electron diffraction (via transmission electron microscopy) of powder X-ray diffraction (or both; Table 4).

6 Spectroscopy

6.1 Raman spectroscopy

The Raman spectrum of kayupovaite (Fig. 6) was obtained from an unpolished sample by means of a LabRam HR800 (Horiba, Japan) spectrometer equipped with an Ar⁺ laser $(\lambda = 514.5 \text{ nm})$ with maximum power of 50 mW and an BX41 microscope (Olympus, Japan), using a 50× confocal objective. The spectrum was acquired at room temperature in a range of $80-3800 \,\mathrm{cm}^{-1}$ at a resolution of $2 \,\mathrm{cm}^{-1}$. To improve the signal-to-noise ratio, the time of acquisition is 150–300 s, and the spectra were repeated three times for each of the three grains. The grains were randomly oriented. The power at the sample was 5 mW. The spectrum contains the following bands (cm $^{-1}$): 3635 and 3560 (O– H stretching vibrations of OH groups and H₂O molecules); 1041, 768, 742, and 717 (Si-O and Al-O stretching modes); 657, 532, 499, 460, 405, 374, and 333 (Mn-O stretching and Si-O-Si modes); and 304, 291, 224, 157, and 100 (lattice modes). The band assignments were made by analogy with the Raman spectra of stilpnomelane and other structurally related phyllosilicates (Kuebler, 2013; Wang et al., 2015). The kayupovaite spectrum is similar to the bannisterite spectrum (R060817) from the RRUFF database (https:

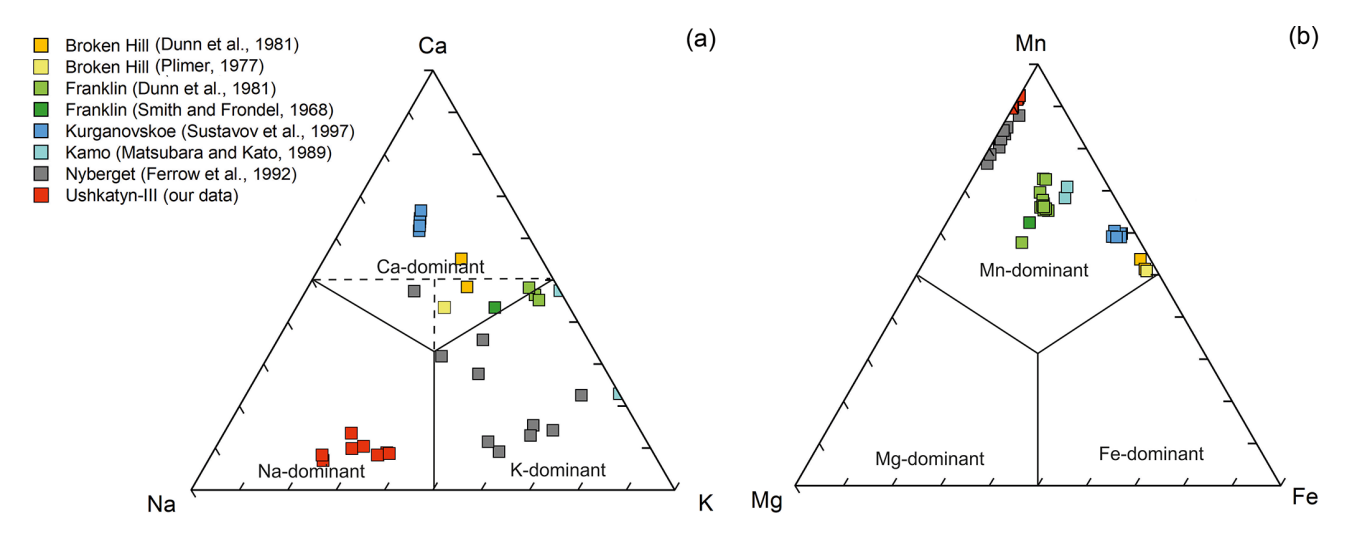


Figure 3. Ratios of interlayer (a) and octahedrally coordinated (b) cations in kayupovaite and bannisterite.

Table 4. Selected crystallographic data for kayupovaite and other stilpnomelane-related minerals.

Name	Sp. gr.	a, Å	b, Å	c, Å	α , $^{\circ}$	β , $^{\circ}$	γ, °	V, Å ³	Z	Reference
Kayupovaite	C2/c	24.915	16.434	22.397	90	94.41	90	9144	8	This study
Bannisterite (Broken Hill)*	C2/c	24.575	16.386	22.286	90	94.36	90	8948	8	Heaney et al. (1992)
Bannisterite (Franklin)*	C2/c	24.668	16.368	22.265	90	94.29	90	8965	8	
Stilpnomelane	$P\bar{1}$	21.724	= b	17.740	121.14	95.86	120	5074	6	Eggleton (1972)
Lennilenapeite	$P1$ or $P\bar{1}$	21.9	_	_	_	_	_	_	1	Dunn et al. (1984)
Franklinphilite	$P1$ or $P\bar{1}$	5.521	9.560	36.57	_	_	_	1930	3/8	Dunn et al. (1992)
Parsettensite	C2/m	39.1	22.84	17.95	90	121.5	90	11216	2	Eggleton and Guggenheim (1994)
Armbrusterite	C2/m	7.333	23.539	13.490	90	115.07	90	4985	2	Yakovenchuk et al. (2007)
Middendorfite	$P2_1/m$ or $P2_1$	12.55	5.721	26.86	90	114.04	90	1761	2	Pekov et al. (2007)

^{*} Authors' parameters were permuted to conform to the standard C2/c setting; - denotes not given.

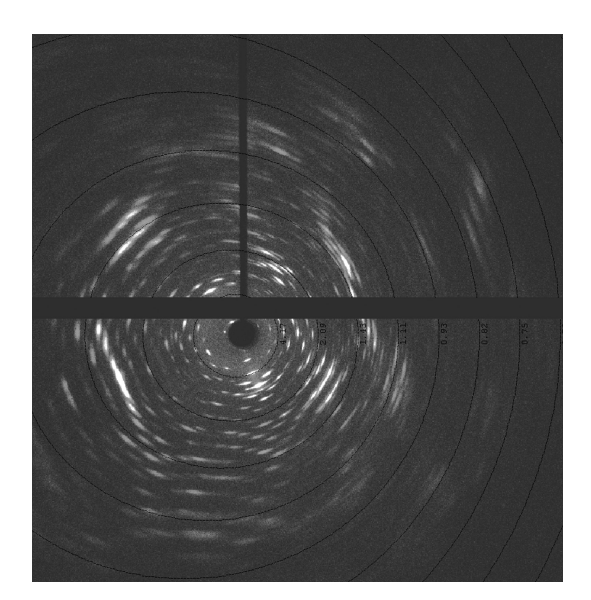


Figure 4. A typical narrow (0.2°) single-crystal frame of kayupovaite.

//rruff.info/bannisterite/, last access: 3 July 2025) and the spectrum of co-type bannisterite from Broken Hill (NSW, Australia) obtained in this work (Fig. 7).

6.2 Infrared spectroscopy

The infrared (IR) absorption spectrum of kayupovaite (Fig. 8) was obtained for a powdered sample mixed with anhydrous KBr and pelletized. The pellet was analyzed using the IR Fourier spectrometer Vertex 70 (Bruker, USA). The spectrum was recorded to be in a range of 400–4000 cm⁻¹. The IR spectrum of kayupovaite is similar to the spectrum of bannisterite (Sustavov et al., 1997) and contains the following bands (cm⁻¹): 3629, 3511, and 3390 (O-H stretching vibrations of OH groups and H₂O molecules); 1640 (H₂O bending vibrations); 1020 (Si–O stretching vibrations); 778 (IVAl-O stretching vibrations); 724 (Mn-O-H bending mode); 651 (O-Si-O bending mode); and 459 (Mn²⁺-O stretching vibrations). The bands near 1400 and 860 cm⁻¹ correspond to stretching and bending vibrations, respectively, of C-O in admixed Mn-rich calcite. The main differences between the IR spectra of bannisterite and kayupovaite from the spectra of other stilpnomelane-related minerals are

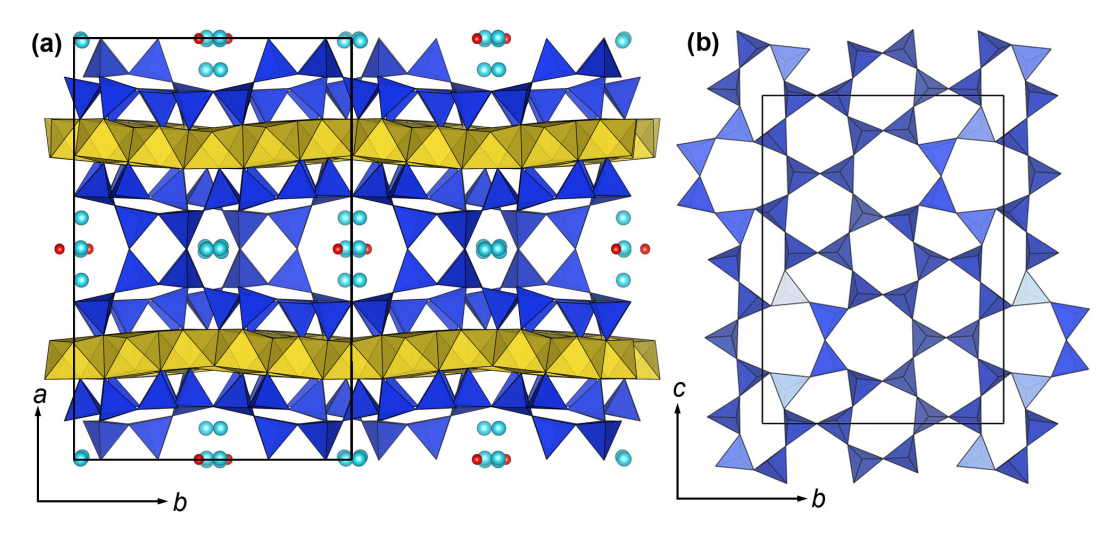


Figure 5. Crystal structure of kayupovaite. (a) Layers composed of edge-sharing $[MnO_6]$ octahedra (yellow) interleaved with a complex of layers of $[SiO_4]$ tetrahedra (blue). Sodium atoms (blue) and water molecules (oxygen atoms of red color) reside in the cavities of the $[SiO_4]$ -based layer. (b) Arrangement of $[SiO_4]$ -based layer adjoined to the layer of $[MnO_6]$ octahedra.

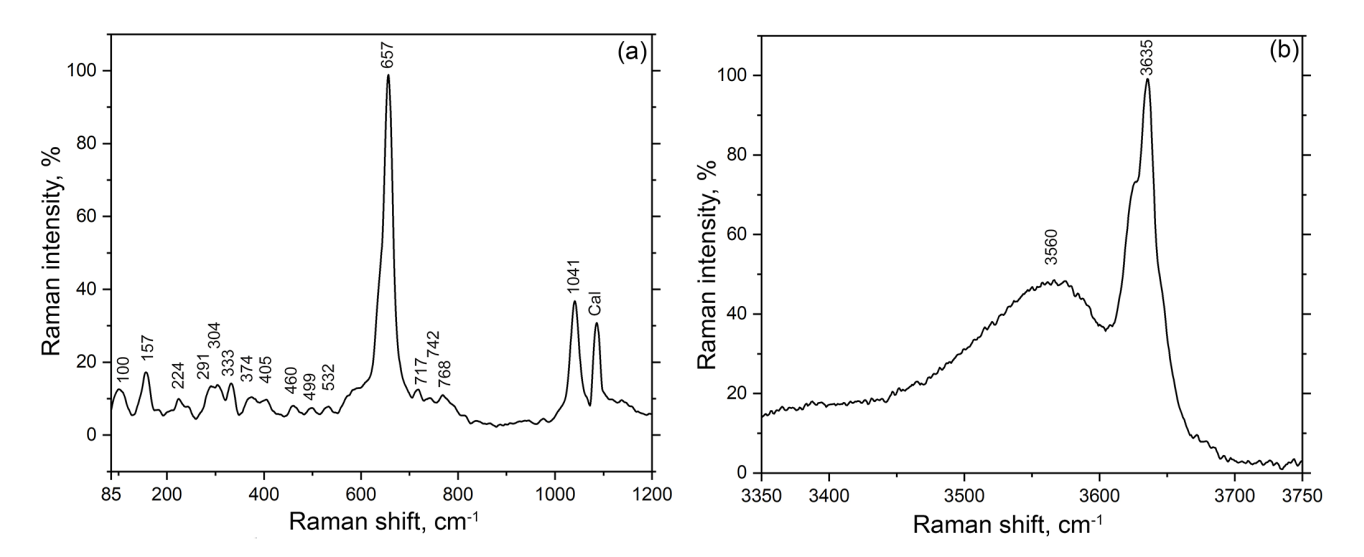


Figure 6. Raman spectrum of kayupovaite. (a) The "fingerprint" region. (b) O-H stretching region. Note: Cal refers to the band corresponding to admixed calcite.

in the region of O–H stretching vibrations $(3000-4000 \,\mathrm{cm}^{-1})$ (Fig. 9).

7 Discussion and conclusions

Kayupovaite stands out among other stilpnomelane-related minerals due to its chemical composition. It is the first mineral of this group that is, in fact, Fe-free: kayupovaite does not contain EDX-detectable iron. In this regard, it is closer to the minerals from peralkaline pegmatites, namely armbrusterite and middendorfite, which contain less than 1 wt % FeO_{tot} (Pekov et al., 2007; Yakovenchuk et al., 2007). The similarity in terms of the ionic radii of Mn and Fe (Shannon, 1976) and the high concentrations of iron $_t$ in bannis-

terite (> 5 wt %; e.g., Plimer, 1977; Heaney et al., 1992; Sustavov et al., 1997) indicate that Fe may be incorporated into the kayupovaite structure. Therefore, the formation of the Fe-free kayupovaite can only be caused due to geochemical and/or mineralogenetic reasons, probably the fractionation of iron and manganese in the mineral-forming medium. This fractionation could have occurred during the formation of the host rock (general depletion of braunite strata in iron) or directly in the process of kayupovaite formation (due to the instability of iron complexes; e.g., Vereshchagin et al., 2025). The absence of a large number of iron minerals and its total low content in braunite-rich ores (e.g., Brusnitsyn et al., 2025) indicate that the most likely version is the separation of manganese from iron during the formation of brau-

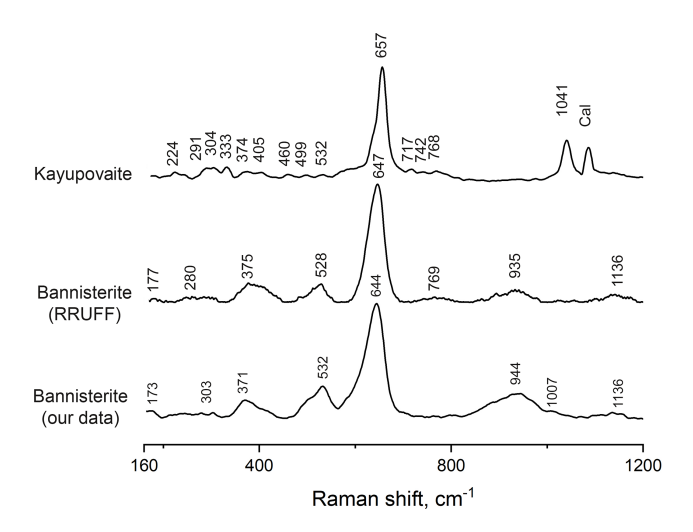


Figure 7. Raman spectra of kayupovaite and bannisterite. Note: Cal denotes calcite.

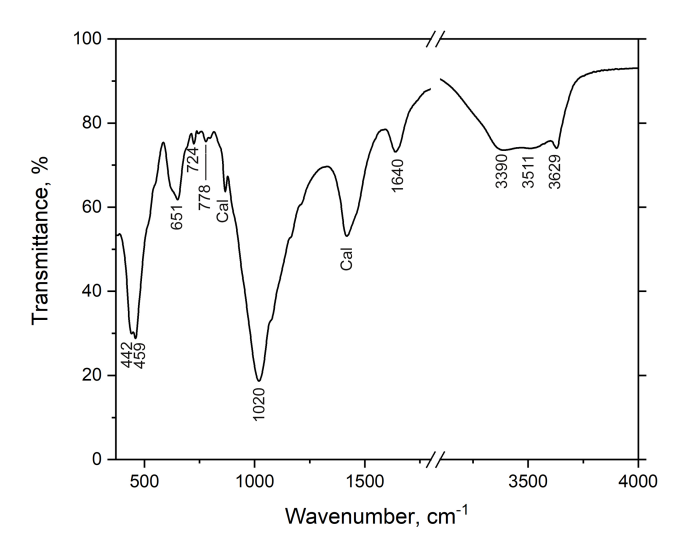


Figure 8. Infrared spectrum of kayupovaite. Note: Cal denotes the band corresponding to admixed calcite.

nite ores. We suggest that the change in oxidation–reduction conditions led to the formation of the Mn-rich and Fe-poor sediments from which kayupovaite was formed. The different degree of oxidation–reduction conditions in hausmannite and braunite ores is, in turn, associated with different concentrations of organic matter, which acted as the main reducing agent. The color of the mineral (light gray), which is not typical for manganese silicates, is also probably a consequence of the absence of iron in the mineral (as, for example, in davreuxite (Fransolet et al., 1984)).

The second striking distinctive chemical feature of kayupovaite is the high sodium content (Na $> K \gg Ca$). Such high Na contents are also not typical for stilpnomelane-related minerals (with the same two exceptions – armbrusterite and middendorfite). Based on the mineralogy of the

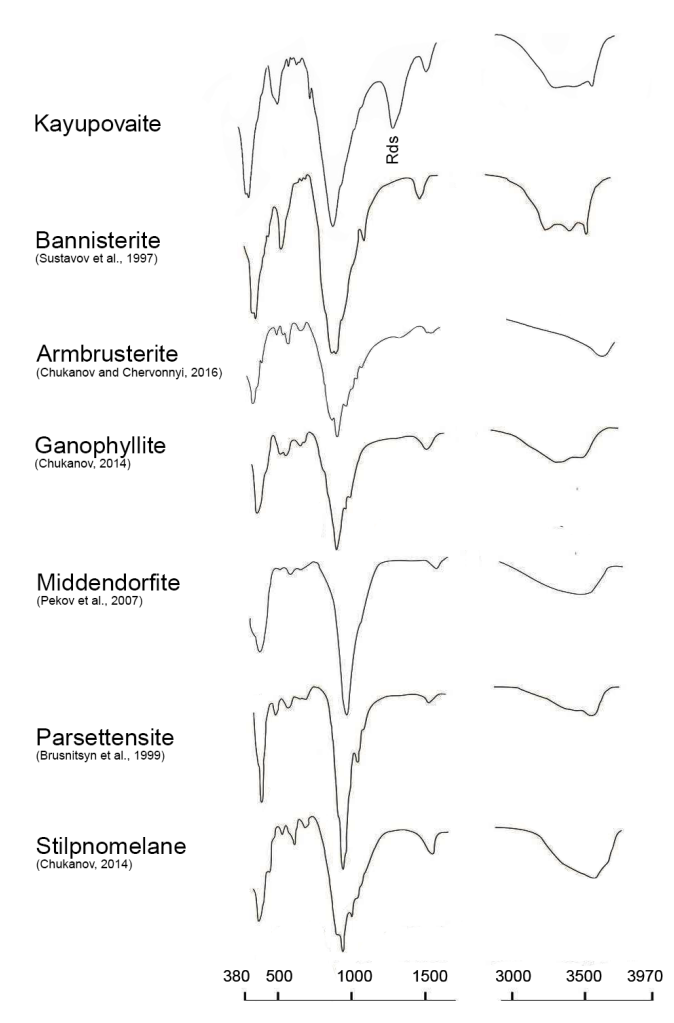


Figure 9. Infrared spectra of kayupovaite, bannisterite, armbrusterite, ganophyllite, middendorfite, parsettenite, and stilpnomelane. Note: Cal denotes the band corresponding to admixed calcite.

deposit and the proposed geological models (e.g., Brusnit-syn et al., 2021, 2024, 2025), we assume that kayupovaite enrichment in sodium is associated with the role of seawater in the formation of manganese-rich sediments. It is most likely that Na was initially present in the form of highly hydrated sodium oxides or silicates (e.g., birnessite, magadiite, or nontronite). Bottom saline solutions, which are characterized by similar Na/K ratios, were the source of sodium for the formation of kayupovaite.

Thermal studies of kayupovaite (TG-DSC) indicate that the mineral is unstable at high temperatures and begins to deteriorate at temperatures below 150 °C. Thus, the presence of kayupovaite indicates a relatively low temperature of rock formation and the absence of the secondary re-heating. It has been shown previously that stilpnomelane is stable up to $\sim 400\text{--}500\,^{\circ}\text{C}$ and 5–6 kbar and will decompose to biotite and almandine at high temperatures and to zussmanite and chlorite at higher pressures (Miyano and Klein, 1989). Thus, we suggest considering all stilpnomelane-related minerals to

be indicators of the low temperatures of formation of their parent rocks. At the same time, individual features of the chemical composition dictate the motive of the crystal structure (e.g., Zagalskaya and Litvinskaya, 1973; Liebau, 1985) and indicate the primary composition of the sediments.

Data availability. CIF files are deposited in the Supplement. Raw data (e.g., Raman spectra) can be obtained on request.

Supplement. The supplement related to this article is available online at https://doi.org/10.5194/ejm-37-829-2025-supplement.

Author contributions. OSV observed the unknown mineral. OSV, AKS, SNB, and VNB collected and interpreted spectroscopic data. SNB and NVP carried out the X-ray diffraction experiments and executed structural refinements. OSV, VVS, and NSV performed the microprobe analyses. SNB, EYA, and AKS carried out optical studies. OSV, SNB, AIB, and ENP participated in the fieldwork. IVP and AIB provided the samples of bannisterite. OSV, IVP, AIB, and SNB wrote the text, in consultation with all of the authors.

Competing interests. The contact author has declared that none of the authors has any competing interests.

Disclaimer. Publisher's note: Copernicus Publications remains neutral with regard to jurisdictional claims made in the text, published maps, institutional affiliations, or any other geographical representation in this paper. While Copernicus Publications makes every effort to include appropriate place names, the final responsibility lies with the authors. Views expressed in the text are those of the authors and do not necessarily reflect the views of the publisher.

Acknowledgements. This work was carried out using the analytical capabilities of the Resource Centers of Saint Petersburg State University: the Center for X-Ray Diffraction Studies, the Center for Optical and Laser Materials Research, the Geomodel Resource Centre, and the Centre for Microscopy and Microanalysis. XRD studies were done at the Center for X-Ray Diffraction Studies under project no. 125021702335-5. SEM-EDX/WDX and Raman studies were done at the Geomodel Resource Centre under project no. 124032000029-9. A photograph of Maria M. Kayupova was kindly provided by Yulia A. Kayupova (her granddaughter). The authors are grateful to Ian Gray and Henrik Friis for the careful examination of the paper contents and for the positive feedback. The authors express their gratitude to the handling chief editor, Sergey V. Krivovichev, for the editorial handing of this contribution.

Financial support. This research has been supported by the Saint Petersburg State University (grant no. 125021702335-5). Publisher's note: the article processing charges for this publication were not paid by a Russian or Belarusian institution.

Review statement. This paper was edited by Sergey Krivovichev and reviewed by Ian Grey and Henrik Friis.

References

- Brusnitsyn, A. I., Starikova, E. V., Krivovichev, S. V., and Chukanov, N. V.: Ba-parsettensite from manganese deposit Kysyl-Tash (South Ural), Zapiski RMO, 6, 79–90, 1999 (in Russian).
- Brusnitsyn, A. I., Kuleshov, V. N., Sadykov, S. A., Perova, E. N., and Vereshchagin, O. S.: Isotopic composition (δ^{13} C and δ^{18} O) and genesis of manganese-bearing deposits of the Ushkatyn-III deposit, Central Kazakhstan, Lithology and Mineral Resources, 522–548, https://doi.org/10.31857/S0024497X20060026, 2020.
- Brusnitsyn, A. I., Perova, E. N., Vereshchagin, O. S., Britvin, S. N., Platonova, N. V., and Shilovskikh, V. V.: The Mineralogy of Iron and Manganese Ores of the Ushkatyn-III Deposit in Central Kazakhstan, Geol. Ore Deposits 63, 772–792, https://doi.org/10.1134/S1075701521080031, 2021.
- Brusnitsyn, A. I., Vladimirova, D. A., Perova, E. N., Vereshchagin, O. S., and Zhukov, I. G.: Jacobsite as an indicator of genrsis of manganese ore of the Ushkatyn-III deposit (Central Kazakhstan), Zapiski Vserossijskogo mineralogičeskogo obsestva, CLIII, 98–118, https://doi.org/10.31857/S0869605524010063, 2024.
- Brusnitsyn, A. I., Perova, E. N., Vereshchagin, O. S., and Britvin, S. N.: Ushkatyn-III deposit: Ba–Pb, Fe, Mn ores in carbonate sediments of the paleorift, Skifia-print, Saint-Petersburg, Russia, ISBN 978-5-98620-758-2, 2025 (in Russian).
- Buzmakov, E. I., Shibrik, V. I., Rozhnov, A. A., Sereda, V., and Radchenko N. M.: Stratiform iron-manganese and polymetallic deposits of the Ushkatynsky ore field (Central Kazakhstan), Geology of Ore Deposits, 1, 32–46, 1975.
- Chukanov, N. V.: Infrared Spectra of Mineral Species: Extended Library, Springer Geochemistry/Mineralogy Ser, Springer Netherlands, Dordrecht, 11733 pp., ISBN 978-94-007-7127-7, https://doi.org/10.1007/978-94-007-7128-4, 2014.
- Chukanov, N. V. and Chervonnyi, A. D.: Infrared Spectroscopy of Minerals and Related Compounds, Springer International Publishing, Cham, https://doi.org/10.1007/978-3-319-25349-7, 2016.
- Dolomanov, O. V., Bourhis, L. J., Gildea, R. J., Howard, J. A. K., and Puschmann, H.: *OLEX2*: a complete structure solution, refinement and analysis program, J. Appl. Crystallogr., 42, 339–341, https://doi.org/10.1107/S0021889808042726, 2009.
- Dunn, P. J., Leavens, P. B., Norberg, J. A., and Ramik, R. A.: Bannisterite: new chemical data and empirical formulae, Am. Mineral., 66, 1063–1067, 1981.
- Dunn, P. J., Peacor, D. R., and Simmons, W. B.: Lennilenapeite, the Mg-analogue of stilpnomelane, and chemical data on other stilpnomelane species from Franklin, New Jersey, The Canadian Mineralogist, 22, 259–263, 1984.

- Dunn, P. J., Peacor, D. R., and Su, S.-C.: Franklinphilite, the manganese analog of stilpnomelane, from Franklin, New Jersey, Mineral. Rec., 23, 465–468, 1992.
- Eggleton, R. A.: The crystal structure of stilpnomelane. Part II. The full cell, Mineral. Mag., 38, 693–711, https://doi.org/10.1180/minmag.1972.038.298.06, 1972.
- Eggleton, R. A. and Guggenheim, S.: The use of electron optical methods to determine the crystal structure of a modulated phyllosilicate: Parsettensite., Am. Mineral., 79, 426–437, 1994.
- Ferrow, E. A., Morad, S., Koark, H. J., and Ounchanum, P.: Bannisterite from the Nyberget Mn-Fe ore deposits, central Sweden. chemistry and mode of occurrence, N. Jb. Miner. Abh., 164, 169–182, 1992.
- Fransolet, A.-M., Abraham, K., and Sahl, K.: Davreuxite: a reinvestigation, Am. Mineral., 69, 777–782, 1984.
- Grice, J. D. and Gault, R. A.: Varennesite, a new species of hydrated Na-Mn silicate with a unique monophyllosilicate structure, Can. Mineral., 33, 1073–1081, 1995.
- Guggenheim, S. and Eggleton, R. A.: Modulated 2:1 layer silicates; review, systematics, and predictions, Am. Mineral., 72, 724–738, 1987.
- Guggenheim, S. and Eggleton, R. A.: Chapter 17. Crystal chemistry, classification, and identification of modulated layer silicates, in: Hydrous Phyllosilicates: (Exclusive of Micas), edited by: Bailey, S. W., Walter de Gruyter GmbH, Boston, 675–718, https://doi.org/10.1515/9781501508998-022, 1988.
- Haugaard, R., Ootes, L., and Konhauser, K.: Neoarchaean banded iron formation within a ~2620 Ma turbidite-dominated deepwater basin, Slave craton, NW Canada, Precambrian Research, 292, 130–151, https://doi.org/10.1016/j.precamres.2017.01.025, 2017.
- Hawthorne, F. C., Uvarova, Y. A., and Sokolova, E.: A structure hierarchy for silicate minerals: sheet silicates, Mineral. Mag., 83, 3–55, https://doi.org/10.1180/mgm.2018.152, 2019.
- Heaney, P. J., Post, J. E., and Evans, H. T.: The Crystal Structure of Bannisterite, Clays Clay Miner., 40, 129–144, https://doi.org/10.1346/CCMN.1992.0400201, 1992.
- Hughes, J. M., Rakovan, J., Bracco, R., and Gunter, M. E.: The atomic arrangement of the ganophyllite-group modulated layer silicates as determined from the orthorhombic dimorph of tamaite, with the elusive 16.8 Å ganophyllite-group superstructure revealed, Am. Mineral., 88, 1324–1330, https://doi.org/10.2138/am-2003-8-915, 2004.
- Kalinin, V. V.: Complex iron-manganese and zinc-lead-barite ores of the Ushkatyn group deposits (Central Kazakhstan), in: Volcanogenic-sedimentary and hydrothermal manganese deposits, Nauka, Moscow, 5–64, 1985.
- Kayupova, M. M.: Pyrosmalite from the Dzhumart and Ushkatyn deposits, central Kazakhstan, Doklady Akademii Nauk USSR, Earth Science Section, 159, 82–85, 1964.
- Kayupova, M. M.: Discovery of brandtite [in Kazakhstan], first one in the USSR, Doklady Akademii Nauk USSR, Earth Science Section, 1198–1200, 1972.
- Kayupova, M. M.: Mineralogy of iron and manganese ores from West Atasu (Central Kazakhstan), Alma-Ata: Nauka, Almaty, Kazakhstan, 1974.
- Krivovichev, S. V., Yakovenchuk, V. N., Armbruster, T., Pakhomovsky, Y. A., Weber, H.-P., and Depmeier, W.: Synchrotron X-ray diffraction study of the structure of shafranovskite,

- K₂Na₃(Mn,Fe,Na)₄[Si₉(O,OH)₂₇](OH)₂ ·nH₂O, a rare manganese phyllosilicate from the Kola peninsula, Russia, Am. Mineral., 89, 1816–1821, https://doi.org/10.2138/am-2004-11-1228, 2004
- Kuebler, K. E.: A combined electron microprobe (EMP) and Raman spectroscopic study of the alteration products in Martian meteorite MIL 03346, J. Geophys. Res.-Planets., 118, 347–368, https://doi.org/10.1029/2012JE004244, 2013.
- Liebau, F.: Structural Chemistry of Silicates: Structure, Bonding, and Classification, Springer Berlin Heidelberg, Berlin, Heidelberg, https://doi.org/10.1007/978-3-642-50076-3, 1985.
- Matsubara, S. and Kato, A.: A barian bannisterite from Japan, Min. Mag., 53, https://doi.org/10.1180/minmag.1989.053.369.09, 85–87, 1989.
- Miyano, T. and Klein, C.: Phase equilibria in the system K₂O-FeO-MgO-Al₂O₃-SiO₂-H₂O-CO₂ and the stability limit of stilpnomelane in metamorphosed Precambrian iron-formations, Contr. Mineral. and Petrol., 102, 478–491, https://doi.org/10.1007/BF00371089, 1989.
- Pekov, I. V., Chukanov, N. V., Dubinchuk, V. T., and Zadov, A. E.: Middendorfite, $K_3Na_2Mn_5Si_{12}(O,OH)_{36} \cdot 2H_2O$, a new mineral species from the Khibiny pluton, Kola Peninsula, Geol. Ore Deposits, 49, 522–529, https://doi.org/10.1134/S1075701507070069, 2007.
- Plimer, I. R.: Bannisterite from Broken Hill, Australia, Neu. Jb. Mineral., Mh., 11, 504–509, 1977.
- Rozhnov, A. A.: Comparative characteristics of manganese deposits of Atasuisky and Nikopol-Chiatura types, in: Geology and geochemistry of manganese, Nauka, Moscow, 116–121, 1982.
- Shannon, R. D.: Revised effective ionic radii and systematic studies of interatomic distances in halides and chalcogenides, Acta Cryst. A, 32, 751–767, https://doi.org/10.1107/S0567739476001551, 1976.
- Sheldrick, G. M.: A short history of SHELX, Acta Crystallogr. A, 64, 112–122, https://doi.org/10.1107/S0108767307043930, 2008
- Smith, M. L. and Frondel, C.: The related layered minerals ganophyllite, bannisterite, and stilpnomelane, Mineral. Mag., 36, 893–913, https://doi.org/10.1180/minmag.1968.283.036.01, 1068
- Sustavov, S. G., Brusnitsyn, A. I., and Ilina, A. N.: New data of bannisterite, Zapiski VRMO, 5, 64–74, 1997 (in Russian).
- Vereshchagin, O. S., Britvin, S. N., Perova, E. N., Brusnitsyn, A. I., Polekhovsky, Y. S., Shilovskikh, V. V., Bocharov, V. N., van der Burgt, A., Cuchet, S., and Meisser, N.: Gasparite-(La), La(AsO₄), a new mineral from Mn ores of the Ushkatyn-III deposit, Central Kazakhstan, and metamorphic rocks of the Wanni glacier, Switzerland, Am. Mineral., 104, 1469–1480, https://doi.org/10.2138/am-2019-7028, 2019.
- Vereshchagin, O. S., Britvin, S. N., Pankin, D. V., Zelenskaya, M. S., Krzhizhanovskaya, M. G., Kuz'mina, M. A., Vlasenko, N. S., and Frank-Kamenetskaya, O. V.: Andreybulakhite, Ni(C₂O₄)·2H₂O, the first natural nickel oxalate, Eur. J. Mineral., 37, 63–74, https://doi.org/10.5194/ejm-37-63-2025, 2025.
- Wang, A., Freeman, J. J., and Jolliff, B. L.: Understanding the Raman spectral features of phyllosilicates, J. Raman Spectrosc., 46, 829–845, https://doi.org/10.1002/jrs.4680, 2015.

Yakovenchuk, V. N., Krivovichev, S. V., Pakhomovsky, Y. A., Ivanyuk, G. Y., Selivanova, E. A., Men'shikov, Y. P., and Britvin, S. N.: Armbrusterite, $K_5Na_6Mn^3+Mn_{14}^{2+}[Si_9O_{22}]_4(OH)_{10}$ ${}^{4}H_2O$, a new Mn hydrous heterophyllosilicate from the Khibiny alkaline massif, Kola Peninsula, Russia, Am. Mineral., 92, 416–423, https://doi.org/10.2138/am.2007.2200, 2007.

Zagalskaya, Y. G. and Litvinskaya, G. P.: Geometrical Crystallography, Moscow University Press, Moscow, 1973.